International Journal of Heat and Mass Transfer 52 (2009) 1667–1676

Contents lists available at ScienceDirect

International Journal of Heat and Mass Transfer

journal homepage: www.elsevier.com/locate/ijhmt

Magnetoconvection in an enclosure of water near its density maximum with Soret and Dufour effects

N. Nithyadevi, Ruey-Jen Yang *

Department of Engineering Science, National Cheng Kung University, Tainan, Taiwan 70101, ROC

ARTICLE INFO

Article history:
Received 12 May 2008
Received in revised form 8 September 2008
Available online 6 December 2008

ABSTRACT

In this paper, unsteady double-diffusive magnetoconvection of water in an enclosure with Soret and Dufour effects around the density maximum has been numerically investigated. The right vertical wall has constant temperature, θ_c, while left vertical wall is θ_h, with $\theta_h > \theta_c$. The concentration in right wall is maintained lower than left wall ($c_h > c_c$). The remaining horizontal walls are adiabatic. The governing equations are solved by control volume method using SIMPLE algorithm with QUICK scheme. Representative results illustrating the effects of the thermal Rayleigh number, Hartmann number, the direction of magnetic field, density inversion parameter, buoyancy ratio, Schmidt number, and Soret and Dufour parameters on the contour maps of the fluid flow, temperature and concentration as well as the profile of velocity at mid-section of the enclosure are reported. In addition, numerical results for the average Nusselt and Sherwood numbers are presented for various parametric conditions and discussed.

1. Introduction

Natural convection in enclosures of cold water occurs commonly in our environment and in many technological processes. This phenomenon has gained an important research topic in the past decade. Water is an important flow media which has well-known physical properties and high thermal conductivity, hence experimental validations are easy to perform. Hydromagnetic flows, heat and mass transfer have become more important in recent years because of many important applications. For example, in many metallurgical processes which involve cooling of continuous strips or filaments, these elements are drawn through a quiescent fluid. During this process, these strips are sometimes stretched. The properties of the final product depend to a great extent on the rate of cooling. This rate of cooling has been proven to be controlled and, therefore, the quality of the final product by drawing such strips in an electrically conducting fluid subject to a magnetic field.

Davis [1] investigated a bench mark numerical solution on natural convection of air in a square enclosure. Ostrach [2] traced out the rich diversity of natural convection problems in science and technology. The numerous studies have focused extensively on convective flows driven by the density inversion effect (Lin and Nansteel [3], Nansteel et al. [4], Tong and Koster [5], Tong [6], Ho and Tu [7], Hossain and Rees [8], Kandaswamy et al. [9] and Nithyadevi et al. [10]).

The steady-state flow structure, temperature and heat transfer in a square enclosure heated and cooled on opposite vertical walls and containing cold water near its density maximum are investigated numerically by Lin and Nansteel [3]. Nansteel et al. [4] studied the natural convection of cold water in the vicinity of its density maximum in a rectangular enclosure in the limit of small Rayleigh number. They observed that the strength of the counter rotating flow decreases with decreasing aspect ratio. Hossain and Rees [8] studied the natural convection of water near its density maximum in an enclosure with heat generation. In this analysis, when the heat generation parameter is sufficiently strong, the circulation of the flow is reversed.

Studies on double diffusive convection can be classified broadly under two types of configurations: in the first type, the fluid is stably stratified by imposing a vertical concentration gradient while the temperature gradient is applied horizontally. In the second one, both the temperature and concentration gradients are imposed laterally. Several studies have been reported in this field (Sezai and Mohamad [11], Blums [12], Hajri et al. [13] and Sivasankaran and Kandaswamy [14]).

Many works have been reported on the flow with heat and mass transfer in the presence of a magnetic field with various aspects. Singh and Cowling [15] studied the convection of liquid in a horizontal magnetic field. Rudraiah et al. [16] investigated numerically the effect of magnetic field on natural convection in a rectangular enclosure. They found that the effect of the magnetic field decreases the rate of heat transfer. Qi et al. [17] have observed both

* Corresponding author. Tel.: +886 6 2002724; fax: +886 6 2766549.
E-mail addresses: nithyadevin@yahoo.co.in (N. Nithyadevi), rjyang@mail.ncku.edu.tw (R.-J. Yang).

0017-9310/$ - see front matter © 2008 Elsevier Ltd. All rights reserved.
doi:10.1016/j.ijheatmasstransfer.2008.09.016

Nomenclature

Alphabetics

B	uniform magnetic field
B_0	magnitude of **B**
C	dimensional concentration (kg m^{-3})
c_p	specific heat at constant pressure (J kg^{-1} K^{-1})
c_s	concentration susceptibility
D	solutal diffusivity (m^2 s^{-1})
D_f	Dufour parameter
D_m	constant molecular diffusivity
g	acceleration due to gravity (m s^{-2})
k_T	thermal diffusion ratio
L	length of the cavity (m)
Nu	local Nusselt number
$\overline{Nu}$	average Nusselt number
P	pressure (kg m^{-1} s^{-2})
Pr	Prandtl number
R	dimensional density inversion parameter
Ra_c	solutal Rayleigh number
Ra_T	thermal Rayleigh number
Sc	Schmidt number
Sh	local Sherwood number
$\overline{Sh}$	average Sherwood number
S_r	Soret parameter
t	dimensional time
T	dimensionless temperature (K)
u and v	velocity components
U and V	dimensionless velocity components (m s^{-1})
x and y	dimensional coordinates
X and Y	dimensionless coordinates (m)
w	center of the heating location (m)

Greek symbols

α	thermal diffusivity (m^2 s^{-1})
β_T	coefficient of thermal expansion (K^{-2})
β_C	coefficient of solutal expansion (m^3 kg^{-1})
μ	dynamic viscosity
ν	kinematic viscosity (m^2 s^{-1})
θ	temperature
θ_l	maximum density inversion temperature
θ_m	mean fluid temperature
ρ	density (kg m^{-3})
τ	dimensionless time

Subscripts

c	cold wall
h	hot wall
o	reference state

electrically conducting and non-conducting fluids of a magnetic field exerts a magnetization force on all materials. Chamkha and Al-Naser [18] who showed that hydromagnetic double diffusive convection flow of an enclosure with opposing temperature and concentration gradients. The unsteady laminar natural convection flow of an electrically conducting fluid in an enclosure under an externally imposed magnetic field has been investigated numerically by Hossain et al. [19].

Two kinds of problem have been mixtures in enclosures. In the first kind (double-diffusive problems) solutal fluxes are imposed to the system through boundary conditions applied on the walls of the system. In the second kind (Soret-induced convection) molecular chaos generated a cross-diffusion which coupled the mass fraction and temperature gradients in the species and heat fluxes. As consequence, heat fluxes imposed across initially homogeneous mixtures induce mass fraction gradients aligned with, or opposed to, the local temperature gradient. In this study these two effects are considered simultaneously. Thermodiffusion is a subject of intensive research due to its wide range of applications in many engineering and technological areas. These include geophysics, oil reservoirs, multi-component melts and storage of nuclear wastes and many other applications. Recent experimental studies on the thermodiffusion phenomenon proved the existence of mixtures (ferrofluids, polymers, sodium chloride in compact clays, etc.) for which the Soret coefficient is large enough to affect considerably the flow and heat and mass transfer in these mixtures. As greater demands are made for tighter control of industrial process, second order effects such as Soret and Dufour diffusion must be considered.

Only a few studies are reported in the literature concerning heat and mass transfer in convection with Soret and Dufour parameters like: Joly et al. [20], Bahloul et al. [21], Postelnicu [22], Plattern [23], Chamkha and Ben-Nakhi [24] and El-Aziz [25]. This study is to obtain a fundamental understanding of natural convection heat and mass transfer characteristics of the effects of the density extermum of water under the Soret and Dufour effects. Particular interest is focused on the heat and mass transfer characteristics due to the magnetic field.

2. Problem formulation

Consider unsteady double diffusive natural convection in a square enclosure of length, L, filled with water in the presence of magnetic field as shown in Fig. 1. Different temperature and concentrations are imposed between the left (θ_h, c_h) and right vertical walls (θ_c, c_c), where the $\theta_h > \theta_c$ and $c_h > c_c$. Adiabatic and impermeable boundary conditions are imposed on the remaining boundaries. The gravity acts in the downward direction. It is also assumed that the enclosure is permeated by a uniform magnetic field, $B = B_x e_x + B_y e_y$ of constant magnitude $B_0 = \sqrt{(B_x^2 + B_y^2)}$, where B_x and B_y are space-independent, e_x and e_y are unit vectors in Cartesian coordinate system. $V = ue_x + ve_y$ is the field velocity. The orientation of the magnetic field forms an angle ϕ with horizontal axis, such that $\tan\phi = B_y/B_x$ The electric current, J, and the electromagnetic force, F, are defined by $J = \sigma_e(V \times B)$ and $F = \sigma_e(V \times B) \times B$, respectively.

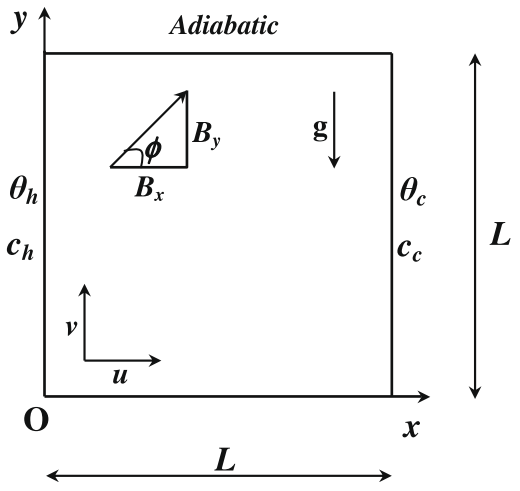

Fig. 1. Physical configuration.

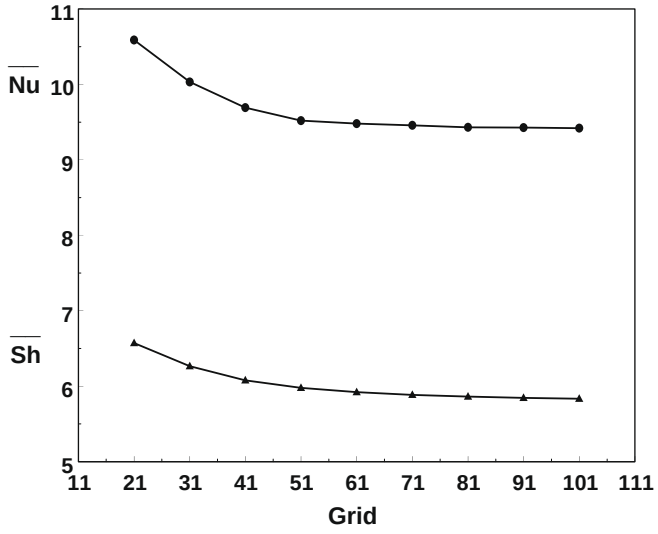

Fig. 2. (a and b) Average Nusselt number and Sherwood number for different grid sizes, $Pr = 11.573$, $Sc = 5$, $Ha = 0$, $N = 0$, $R = D_f = S_r = 0$ and $Ra_T = 10^6$.

The governing equations for two-dimensional laminar incompressible buoyancy-induced flows with the Soret and Dufour effects, Boussinesq approximation and constant fluid properties in a Cartesian coordinate system are:

$$\frac{\partial u}{\partial x}+\frac{\partial v}{\partial y}=0, \tag{1}$$

$$\frac{\partial u}{\partial t}+u\frac{\partial u}{\partial x}+v\frac{\partial u}{\partial y}=-\frac{1}{\rho_0}\frac{\partial p}{\partial x}+\nu\nabla^2 u + \frac{\sigma_e B_0^2}{\rho_0}\left(v\sin\phi\cos\phi-u\sin^2\phi\right) \tag{2}$$

Table 1
Comparison of average Nusselt number for different Rayleigh number in a square cavity with $Pr = 0.7$, $R = N = Sc = D_f = S_r = 0$.

Ra_T	Davis [1]	Hadjisophocleous et al. [27]	Present
10^3	1.118	1.141	1.123
10^4	2.238	2.290	2.304
10^5	4.509	4.964	4.899
10^6	8.810	10.390	10.477

$$\frac{\partial v}{\partial t}+u\frac{\partial v}{\partial x}+v\frac{\partial v}{\partial y}=-\frac{1}{\rho_0}\frac{\partial p}{\partial y}+\nu\nabla^2 v-\frac{\rho}{\rho_0}g + \frac{\sigma_e B_0^2}{\rho_0}\left(u\sin\phi\cos\phi-v\cos^2\phi\right) \tag{3}$$

$$\frac{\partial \theta}{\partial t}+u\frac{\partial \theta}{\partial x}+v\frac{\partial \theta}{\partial y}=\alpha\nabla^2\theta+\frac{Dk_T}{c_s c_p}\nabla^2 c \tag{4}$$

$$\frac{\partial c}{\partial t}+u\frac{\partial c}{\partial x}+v\frac{\partial c}{\partial y}=D\nabla^2 c+\frac{Dk_T}{\theta_m}\nabla^2\theta \tag{5}$$

The following hypotheses are taken for this work. The density of the cold water is assumed to vary with temperature according to the following parabolic relationship. Most of the authors like (Nansteel et al. [3], Tong and Koster [5], Tong [6], and Ho and Tu [7]): $\rho = \rho_o[1-\beta_T(\theta-\theta_l)^2]$, where ρ_o is the maximum density at the temperature $\theta_l = 3.98\ ^\circ C$. But this relation is valid in the temperature range between 0 and 8 °C. This variation, due to both temperature and concentration gradients, can be described by the following equation $\rho = \rho_o[1-\beta_T(\theta-\theta_l)^2+\beta_C(c-c_o)]$ ($\beta_T = 8.0\times10^{-6}\,(^\circ C)\,K^{-2}$, $\beta_C = 3.0\times10^{-3}\,m^3\,kg^{-1}$) where β_T and β_C are the coefficients for thermal and concentration expansions.

The appropriate initial and boundary conditions are:

$$\begin{aligned}
&t=0:\ u=v=0,\ \theta=\theta_c, && c=c_c,\ && 0\leqslant x\leqslant L,\ 0\leqslant y\leqslant L,\\
&t>0:\ u=v=0,\ \tfrac{\partial\theta}{\partial y}=\tfrac{\partial c}{\partial y}=0, && && 0\leqslant x\leqslant L,\ y=0 \text{ and } L,\\
&\quad u=v=0,\ \theta=\theta_h, && c=c_h,\ && x=0,\ 0\leqslant y\leqslant L,\\
&\quad u=v=0,\ \theta=\theta_c, && c=c_c,\ && x=L,\ 0\leqslant y\leqslant L.
\end{aligned}$$

Dimensionless variables are defined as follows:

$$\tau=\frac{t}{L^2/\nu},\quad (X,Y)=\frac{(x,y)}{L},\quad (U,V)=\frac{(u,v)}{\nu/L},\quad P=\frac{pL^2}{\rho_0\nu^2},$$
$$T=\frac{\theta-\theta_c}{\theta_h-\theta_c},\quad C=\frac{c-c_c}{c_h-c_c},\quad \text{with}\quad \theta_h>\theta_c,\quad c_h>c_c.$$

The non-dimensional form of the Eqs. (1)–(5) is obtained as:

$$\frac{\partial U}{\partial X}+\frac{\partial V}{\partial Y}=0, \tag{6}$$

$$\frac{\partial U}{\partial \tau}+U\frac{\partial U}{\partial X}+V\frac{\partial U}{\partial Y}=-\frac{\partial P}{\partial X}+\nabla^2 U + Ha^2[V\sin\phi\cos\phi-U\sin^2\phi] \tag{7}$$

Table 2
Comparison of average Nusselt number for different density inversion parameters with $Pr = 11.67$, $N = Sc = D_f = S_r = 0$.

Ra_T	$R = 0.5$			$R = 1.0$		
	Tong [5]	Lin and Nansteel [3]	Present	Tong [5]	Lin and Nansteel [3]	Present
10^3	1.0007	1.0009	1.1167	1.1186	1.119	1.176
10^4	1.0655	1.076	1.0750	2.2739	2.278	2.289
10^5	2.0298	2.080	2.0409	4.7143	4.709	4.800
10^6	4.0272	4.090	4.1174	9.2742	9.195	9.123

Table 3
Comparison of average Nusselt number for different Hartmann numbers and magnetic force with $Pr = 1$, $R = N = Sc = D_f = S_r = 0$.

Gr	$Ha = 0$		$Ha = 100$			
	Ece and Buyuk [28]	Present	$\phi = 0^o$		$\phi = 90^o$	
			Ece and Buyuk [28]	Present	Ece and Buyuk [28]	Present
10^3	3.745834	3.722434	3.681442	3.680664	3.678740	3.650668
10^4	4.771623	4.752022	3.683067	3.681597	3.681277	3.653205
10^5	6.677280	6.647159	3.824211	3.815782	3.885215	3.865714
10^6	–	10.100202	6.766862	6.749894	–	7.025964

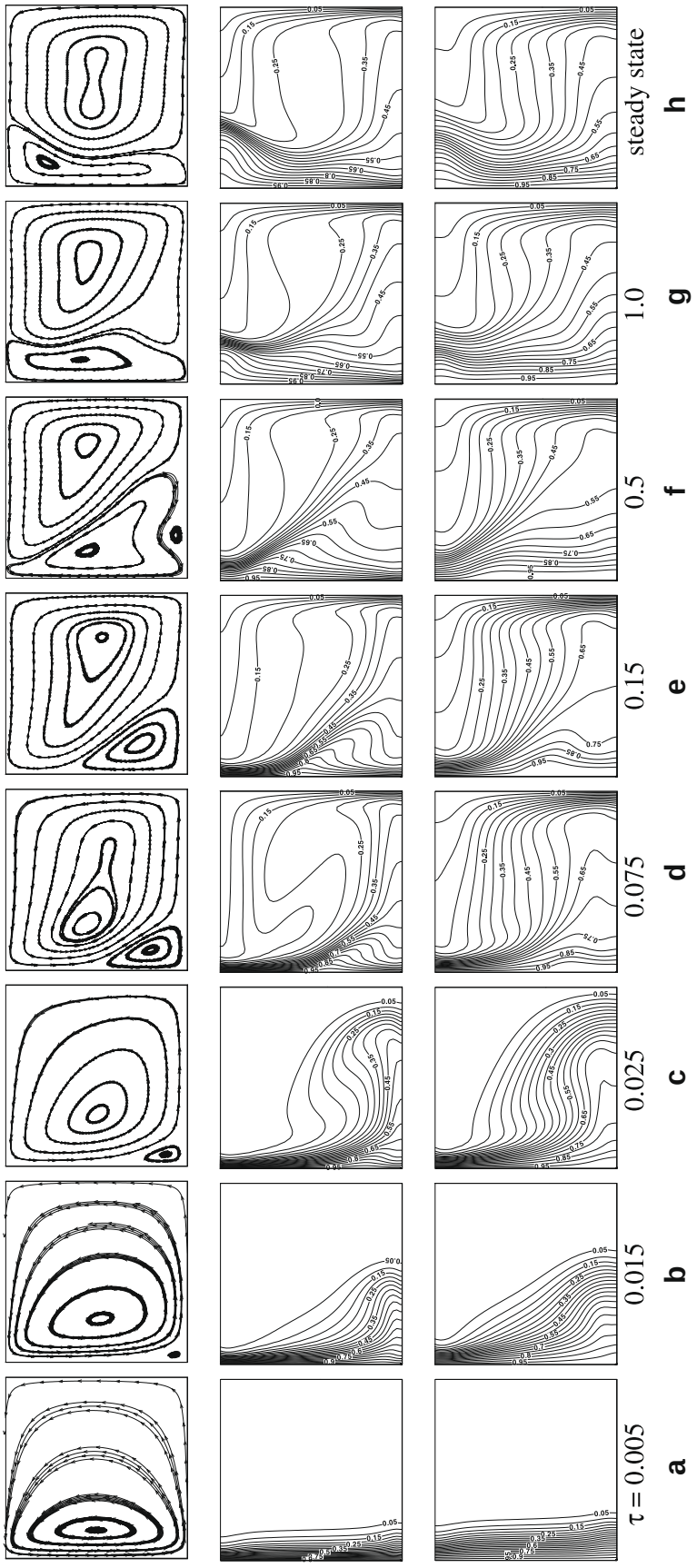

Fig. 3. (a–h) Transient state of streamlines, isotherms and iso-concentration for $R = 0.2$, $N = 0.5$, $Ha = 10$, $\phi = 30^{o}$, $D_f = S_r = 0.5$ and $Ra_T = 10^6$.

$$\frac{\partial V}{\partial \tau}+U\frac{\partial V}{\partial X}+V\frac{\partial V}{\partial Y}=-\frac{\partial P}{\partial Y}+\nabla^2 V+\frac{Ra_T}{Pr}[(T-R)^2-NC]+Ha^2[U\sin\phi\cos\phi-V\cos^2\phi] \quad (8)$$

$$\frac{\partial T}{\partial \tau}+U\frac{\partial T}{\partial X}+V\frac{\partial T}{\partial Y}=\frac{1}{Pr}\nabla^2 T+D_f\nabla^2 C \quad (9)$$

$$\frac{\partial C}{\partial \tau}+U\frac{\partial C}{\partial X}+V\frac{\partial C}{\partial Y}=\frac{1}{Sc}\nabla^2 C+S_r\nabla^2 T \quad (10)$$

The initial and boundary conditions that solve the stated problem are:

$$\begin{aligned}
&\tau=0:\ U=V=0,\ T=C=0, && 0\leqslant X\leqslant 1,\ 0\leqslant Y\leqslant 1,\\
&\tau>0:\ U=V=0,\ \tfrac{\partial T}{\partial Y}=\tfrac{\partial C}{\partial Y}=0, && 0\leqslant X\leqslant 1,\ Y=0\&1,\\
&\quad U=V=0,\ T=1, \quad C=1,\ X=0, && 0\leqslant Y\leqslant 1,\\
&\quad U=V=0,\ T=0, \quad C=0,\ X=1, && 0\leqslant Y\leqslant 1.
\end{aligned}$$

The non-dimensional parameters that appear in the equations are: $Ha^2=\frac{\sigma_e B_0^2 L^3}{\mu}$ Hartmann number, $Ra_T=\frac{g\beta T(\theta_h-\theta_c)^2 L^3}{\nu^2}$ thermal Rayleigh number, $Ra_c=\frac{g\beta_c(c_h-c_c)L^3}{\nu^2}$ solutal Rayleigh number, $Pr=\frac{\nu}{\alpha}=11.573$ Prandtl number, $D_f=\frac{Dk_T(c_h-c_c)}{c_s c_p \nu(\theta_h-\theta_c)}$ Dufour parameter, $S_r=\frac{Dk_T(\theta_h-\theta_c)}{\theta_m \nu(c_h-c_c)}$ Soret parameter, $Sc=\frac{\nu}{D}$ Schmidt number, $R=\frac{\theta_1-\theta_c}{\theta_h-\theta_c}$ density inversion parameter, and $N=\frac{Ra_c}{Ra_T}$ Buoyancy ratio number. The local Nusselt number and Sherwood number is defined by $Nu=-\frac{\partial T}{\partial X}|_{X=0}$, $Sh=-\frac{\partial C}{\partial X}|_{X=0}$, resulting in the average Nusselt number and Sherwood number as $\overline{Nu}=\int_0^1 Nu\,dY$ and $\overline{Sh}=\int_0^1 Sh dY$.

3. Numerical scheme

The non-dimensional equations subject to the boundary conditions and for the treatment of the pressure–velocity coupling are integrated over a control volume method, solved by the SIMPLE algorithm of Patankar [26]. The discretizations followed the QUICK scheme. The solution domain consist a number of grid points at which discretization equations are applied. Uniform staggered grid system is employed in the present study. The numerical simulation are carried out for highly accurate solution in the average Nusselt and Sherwood numbers for various grid sizes (21×21–101×101) are presented to develop an understanding of the grid fineness as seen in Fig. 2. There is considerable change in the average Nusselt and Sherwood numbers from 21×21 to 61×61 and no noticeable change is observed from 61×61 to 101×101. Hence considering the uniform grid system of 81×81 is chosen for the calculation of all cases. The mass balance for global convergence is taken as 10^{-7}. Under relaxation technique is employed for the pressure correction. The resulting set of discretized equations for each variable is solved by a line-by-line procedure, combining the tri-diagonal matrix algorithm (TDMA). The accuracy of the aforementioned numerical method is validated by direct comparisons with the numerical results reported earlier by Davis [1], Hadjisophocleous et al. [27], Tong [6], and Lin and Nansteel [3] in the absence of magnetic field and Ece and Buyuk [28] in the presence of magnetic field. Tables 1–3 present the results of these various comparisons. It can be seen from these tables that excellent agreement between the results exists. These favorable comparisons lend confidence in the numerical results to be reported in the next section.

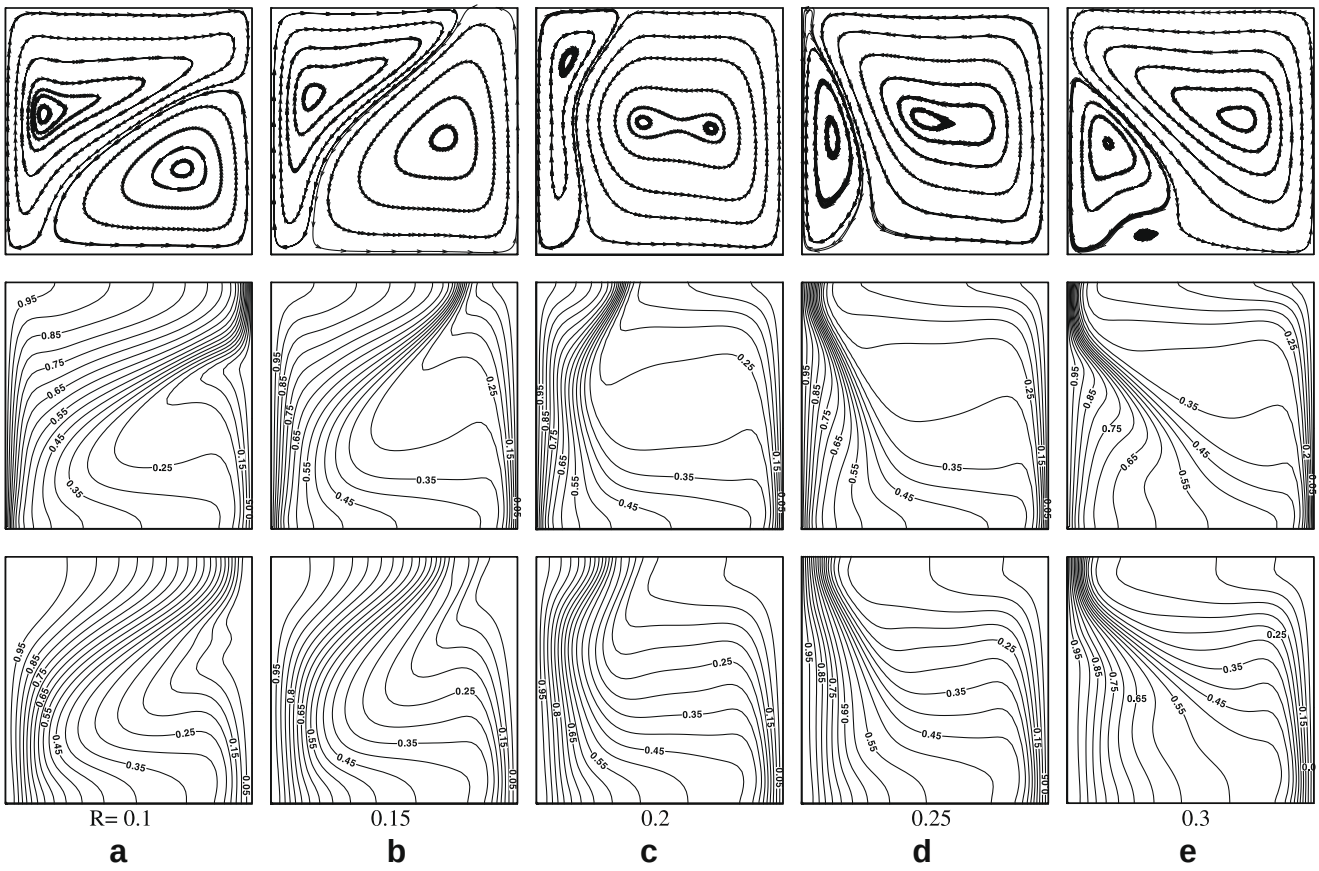

Fig. 4. (a–e) Steady state of streamlines, isotherms and iso-concentration for different R, $Ha=10$, $N=0.5$, $\phi=30^o$, $D_f=S_r=0.5$ and $Ra_T=10^6$.

4. Results and discussion

Numerical study is performed to understand the unsteady double diffusive convection of cold water near its density maximum in an enclosure with Soret and Dufour parameters in the presence of a magnetic field. Computations are carried out for the Prandtl number, Pr (=11.573), the thermal Rayleigh number, Ra_T (=10^3–10^6), the Hartmann number, Ha (=0–100), the buoyancy ratio number, N (=0.2–0.8), the density inversion parameter, R (=0.1–0.3), the Schmidt number, Sc (=5), Soret and Dufour parameters, S_r and D_f (=0–1). Typical value of direction of the external magnetic field with the horizontal considered to be ϕ (=0^o, 30^o, 60^o, and 90^o). The results are presented as streamlines, isotherms and isoconcentrations. The rate of heat and mass transfer in the enclosure is measured in terms of the average Nusselt and Sherwood numbers.

Fig. 3(a–h) illustrate the transient-state streamlines, isotherms and isoconcentrations for R = 0.2, $N = 0.5$, $Ha = 10$, $\phi = 30^o$, $D_f = S_r = 0.5$ and $Ra_T = 10^6$. At the very beginning of the process, a small amount of fluid near the heating wall is activated so as to produce a small buoyancy-induced anticlockwise rotating cell. The corresponding isotherms and isoconcentrations are parallel to the vertical wall near the hot location and the transfer of heat is through conduction. As time progresses a secondary clockwise rotating convective cell exists due to the density inversion of water near the left bottom corner. Further as time evolves, the secondary cell grows in its size to occupy nearly one-third of the enclosure slightly suppressing the cold convective cell, evidencing the density maximum behavior of water. The isotherms and isoconcentrations gradually spread over the whole enclosure.

Fig. 4(a–e) indicate the flow, energy and mass patterns for different density inversion parameter at Hartmann number 10, $N = 0.5$, $D_f = S_r = 0.5$, $Ra_T = 10^6$ and for the nearly diagonal magnetic field $\phi = 30^o$. When $R = 0$ there is no density inversion inside the enclosure which results a single cellular flow pattern with hot fluid raises along the hot wall and cool fluid downs along the cold wall (not included in this figure). When increasing R, there exists a density inversion inside the enclosure. A dual cell pattern appears inside the enclosure in all cases due to the inversion of density of water. For low-density inversion parameter, a cold cell rotating in the counter clockwise direction rising along the cold wall and dropping along the hot cell and the hot cell rotates clockwise direction which appears within the enclosure. A pair of counter rotating cells of almost equal strength appears with maximum density

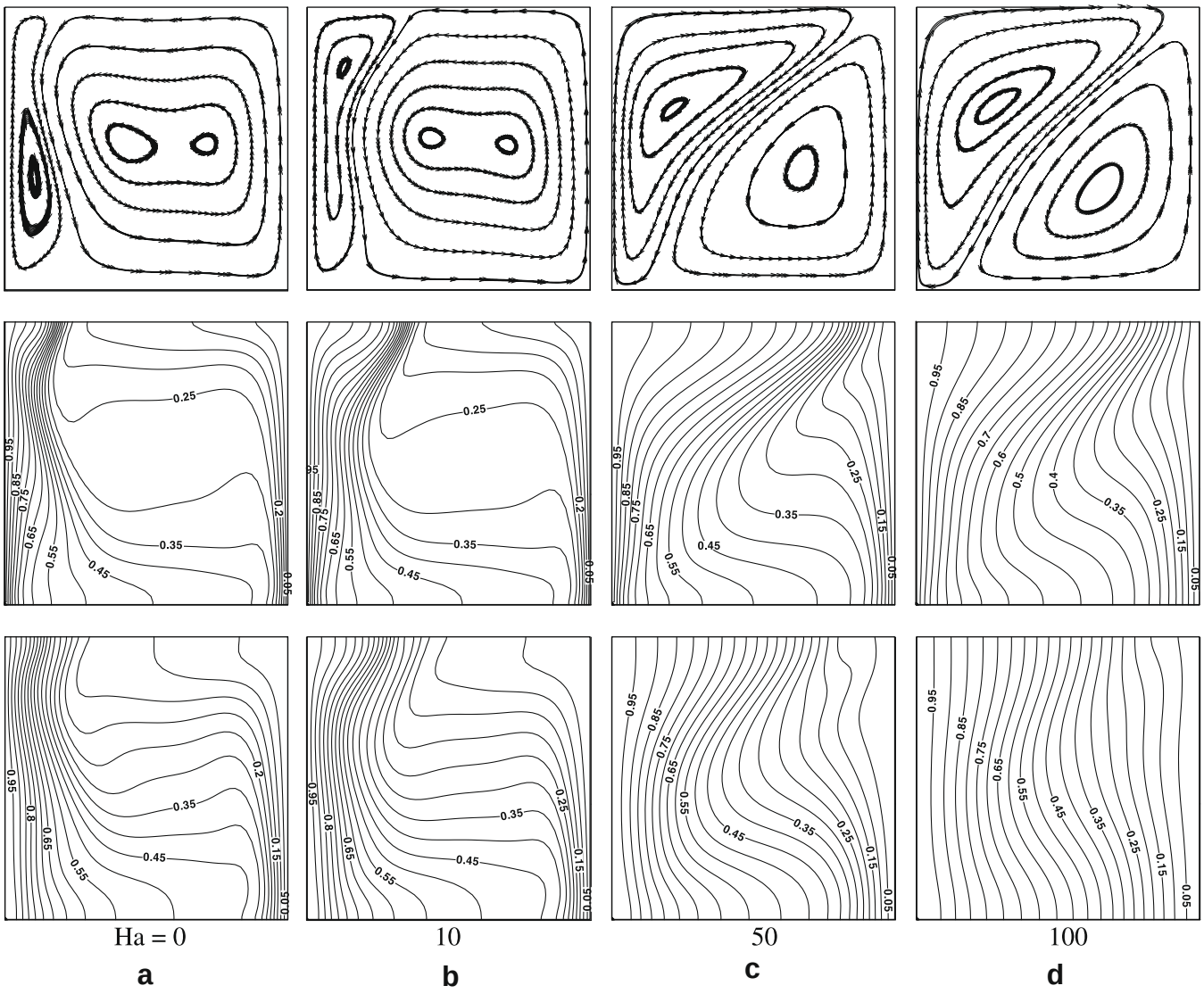

Fig. 5. (a–d) Steady state of streamlines, isotherms and iso-concentration for different Hartmann numbers, $R = 0.2$, $N = 0.5$, $\phi = 30^o$, $D_f = S_r = 0.5$ and $Ra_T = 10^6$.

plane at the center of the enclosure due to the anomalous density expansion of water at that temperature. At this stage the convection mode of heat transfer is suppressed completely and conduction mode is dominant of heat transfer. As the density inversion parameter increase the strength of the primary cell is reduced and pushed to the left bottom corner of the enclosure and the secondary cell once again gains its strength and occupies the three-fourth of the enclosure indicating the establishment of convective mode of heat transfer and introduces thermal boundary layer at the left top and right bottom of the enclosure. The maximum density plane moves from cold wall side to hot wall side in the isotherms and isoconcentrations when increasing the density inversion parameter.

In Fig. 5(a–d) the steady-state streamlines, isotherms and isoconcentrations are depicted for the effect of Hartmann numbers while the magnetic field applied in the direction diagonal with $R = 0.2$, $N = 0.5$, $D_f = S_r = 0.5$ and $Ra_T = 10^6$. In this figure, we see the presence of two-cell pattern. The intensities in both the primary and secondary flow decrease owing to the increase in the magnetic field. The corresponding effect of the increase in Hartmann number on the isotherms and iosconcentrations are that they are more vertical and straighten out since the magnetic field resists the flow and the convection is totally suppressed inside the enclosure. For sufficiently large Hartmann number in density maximum region the convection is completely suppressed. In such situation the heat and mass transfer is dominated by conduction. When increasing the Hartmann number the heat and mass transfer rate is decreased for all directions of external magnetic field. This effect can also be seen in Fig. 6(a and b).

Fig. 6(a and b) show the average Nusselt and Sherwood numbers for different thermal Rayleigh number with different Hartmann number. Increasing Hartmann number decreased the heat and mass transfer rate. In such situation the heat transfer is dominated by conduction. When the thermal Rayleigh number increases the average Nusselt number also increases, but the heat transfer rate is high in $Ha = 0$. The mass transfer rate is decreased for high Hartmann number when increasing the thermal Rayleigh number.

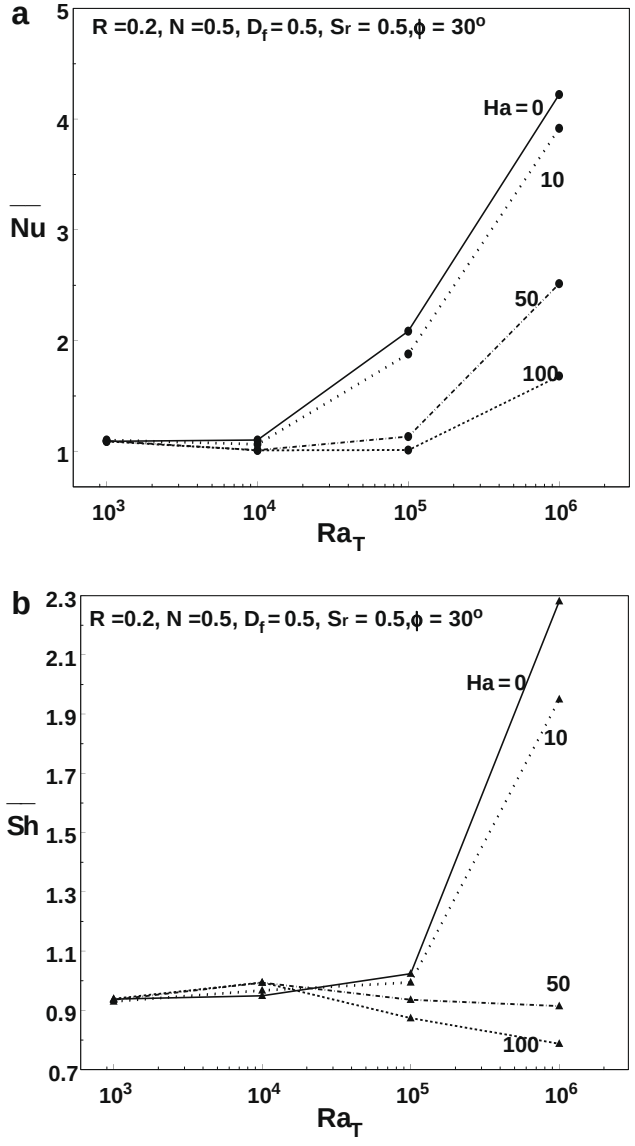

Fig. 6. (a and b) Average Nusselt number and Sherwood number vs thermal Rayleigh number for different Hartmann number, $R = 0.2$, $N = 0.5$, $\phi = 30^o$ and $D_f = S_r = 0.5$.

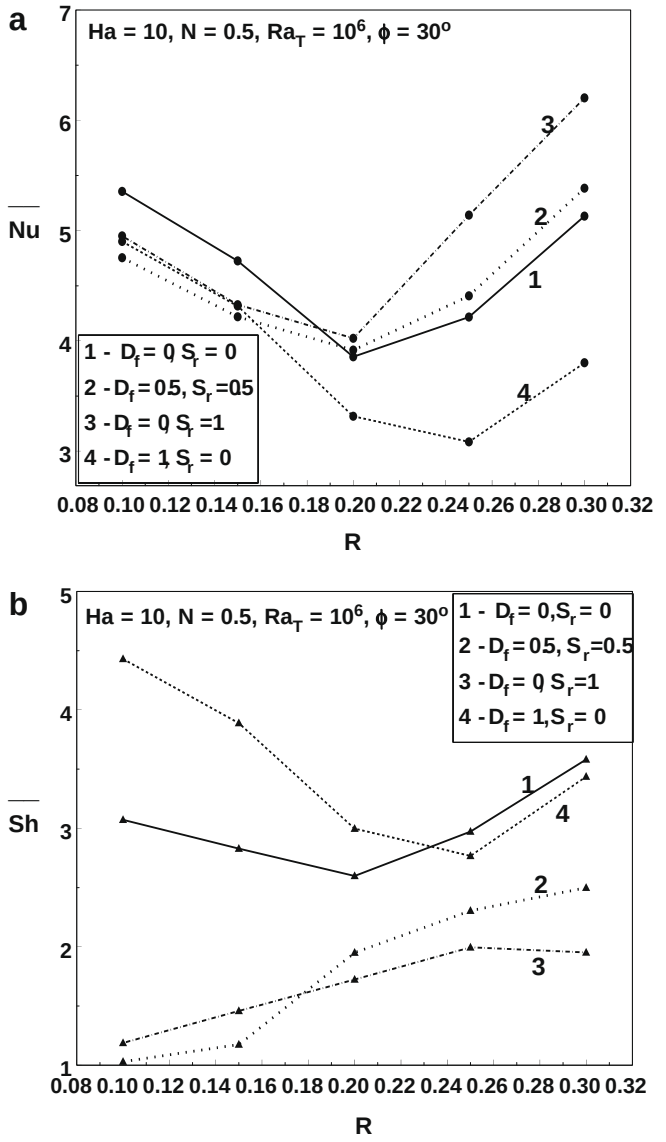

Fig. 7. (a and b) Average Nusselt number and Sherwood number vs R for different Dufour and Soret parameters, $Ha = 10$, $N = 0.5$, $\phi = 30^o$ and $Ra_T = 10^6$.

Fig. 7(a and b) illustrate that the average heat and mass transfer vs density inversion R with different Soret and Dufour parameters. The fall in the heat and mass transfer rate is due to the effect of density maximum. The same effect of density maximum on heat and mass transfer for various values of R is observed in the case of different values of Soret and Dufour parameter. But in Fig. 7(b) the mass transfer rate behaviors differently in the presence of Soret parameter. $D_f = 1$, $S_r = 0$ and $D_f = 0$, $S_r = 0$ gives better mass transfer rate and low heat transfer rate but the opposite of it holds for $D_f = 0.5$, $S_r = 0.5$ and $D_f = 0$, $S_r = 1$. The average Nusselt number and Sherwood number for different Ha with different values of direction of external magnetic field ϕ are displayed in Fig. 8(a and b). It is seen from Fig. 8(a) that the heat transfer rate is minimum when $\phi = 0^o$, that is horizontal magnetic field. Heat transfer is enhanced when the angle of external magnetic field $\phi = 90^\circ$. But in Fig. 8(b) that the mass transfer rate is clear that the opposite of the above holds.

The average Nusselt number and Sherwood number for different buoyancy ratio with different density inversion parameter, $Ha = 10$, $\phi = 30^\circ$, $D_f = S_r = 0.5$ and $Ra_T = 10^6$ are displayed in Fig. 9(a and b). It is also found that the average Nusselt number and Sherwood number gets minimum in the density maximum region. For such a situation, the dual cell structure inhibits the direct convective transfer of energy from the hot to the cold cell. This phenomenon results essentially from the inversion of the fluid density at 4 °C and is one of its most significant effects on the mechanism of heat transfer by convection of water within an enclosure. So heat transfer rate is reduced in such a situation for all values of density inversion parameter. The heat and mass transfer rate are high for the low N and R. Further increasing N and R the heat and mass transfer also increase.

Fig. 10(a and b) show the behavior of the average Nusselt and Sherwood numbers, for different Hartmann number with different R. In all cases, the heat and mass transfer rate goes down as the Hartmann number increases. The average Nusselt number is very low in the value of $R = 0.3$ in compare to all other values, but in average Sherwood number is clearly observed opposite reaction holds. In Fig. 6–10(a and b) observe that the unity of the vertical scale in the average Nusselt number is two times more than average Sherwood number. The suppression of the

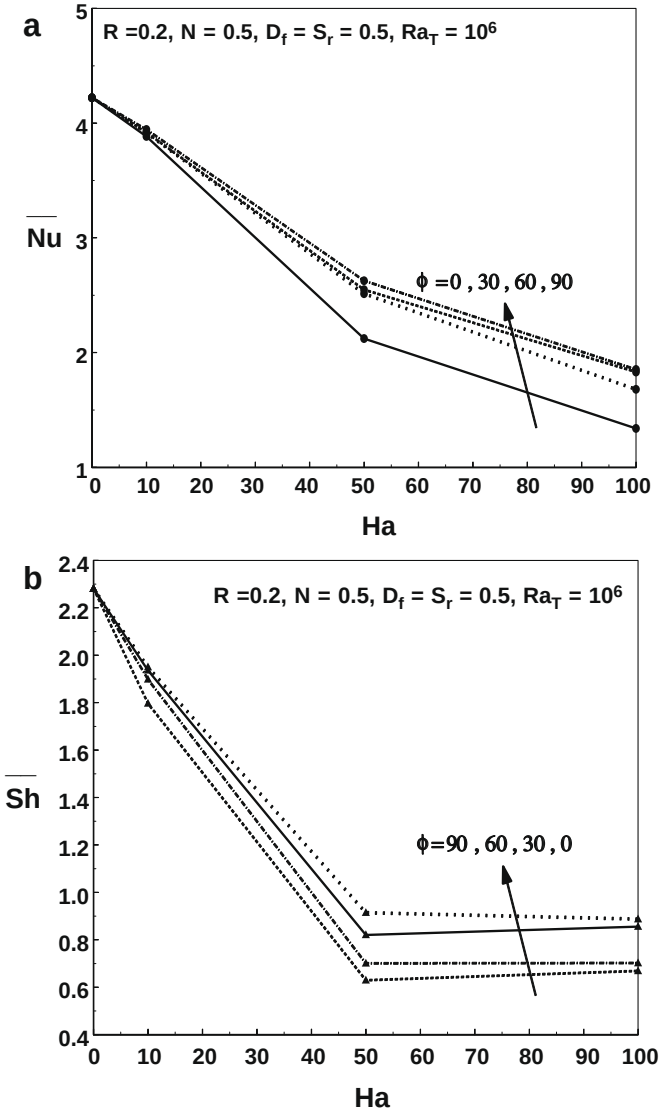

Fig. 8. (a and b) Average Nusselt number and Sherwood number vs Hartmann numbers for different magnitude angle, $R = 0.2$, $N = 0.5$, $D_f = S_r = 0.5$ and $Ra_T = 10^6$.

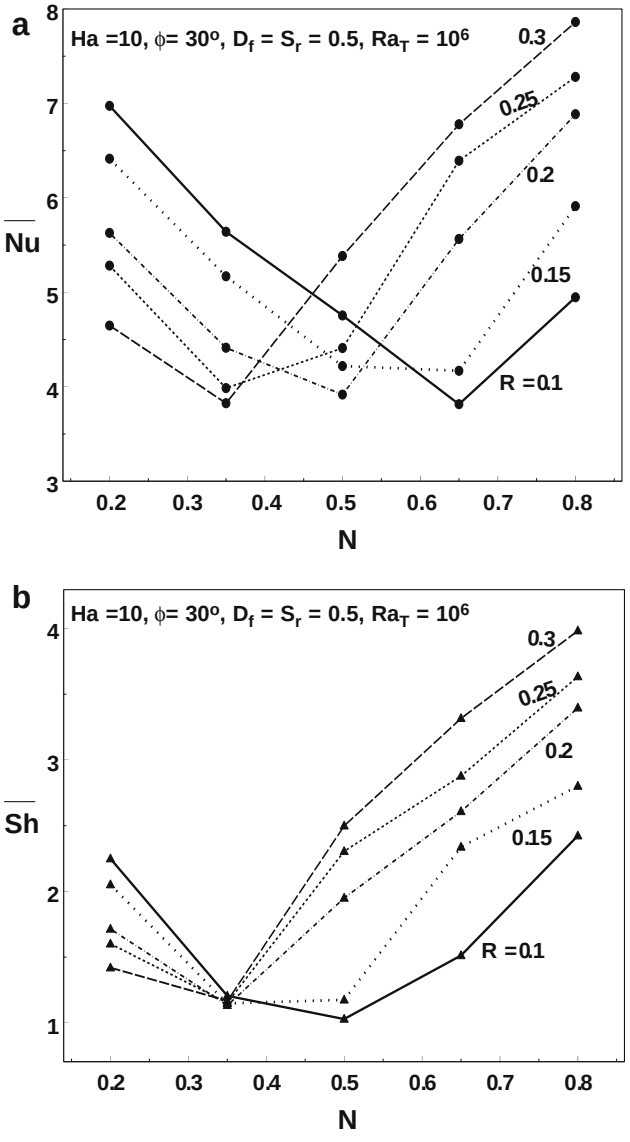

Fig. 9. (a and b) Average Nusselt number and Sherwood number vs N for different R, $Ha = 10$, $\phi = 30^o$, $D_f = S_r = 0.5$ and $Ra_T = 10^6$.

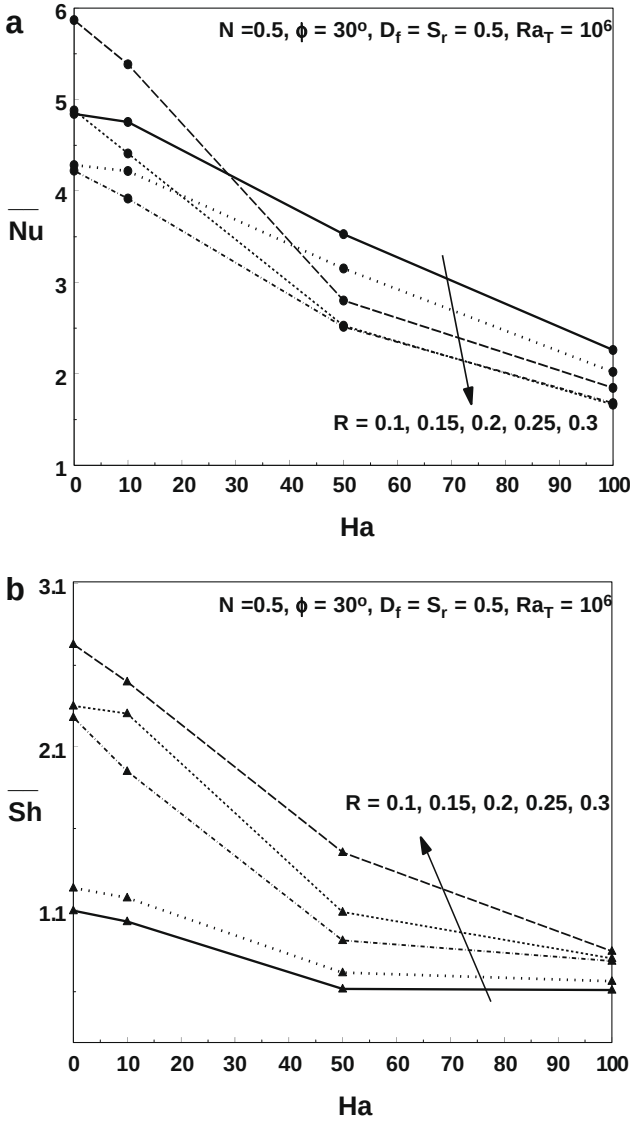

Fig. 10. (a and b) Average Nusselt number and Sherwood number vs Hartmann numbers for different R, $N = 0.5$, $\phi = 30^o$, $D_f = S_r = 0.5$ and $Ra_T = 10^6$.

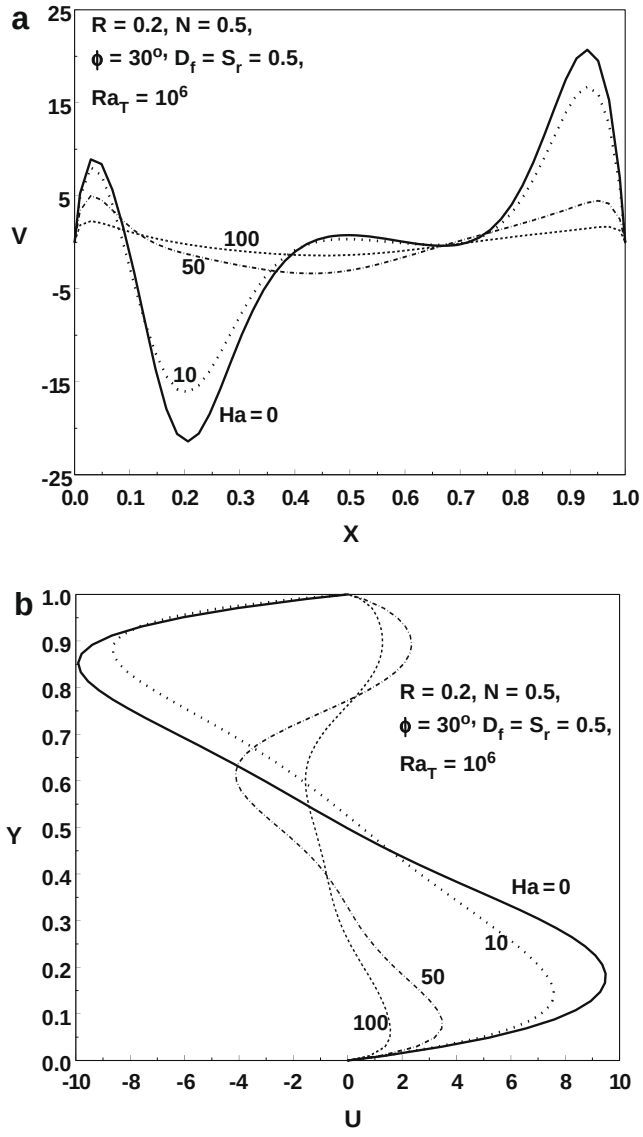

Fig. 11. (a and b) Mid-height vertical and horizontal velocities at the middle of the enclosure for different Hartmann numbers.

velocity field by the magnetic field is also demonstrated in Fig. 11(a and b) by drawing the steady state vertical and horizontal velocities for various values of *Ha*. From these figures, we observe that the velocity field is considerably decreased with the application of the magnetic field. It is clear that with the increase in *Ha*. The profiles are flattened for higher values of the Hartmann number. The velocity in the core region is almost suppressed and the peak velocities are observed near the end walls. The local Nusselt and Sherwood number for different Hartmann numbers, $R = 0.2$, $N = 0.5$, $\phi = 30^o$, $D_f = S_r = 0.5$ and $Ra_T = 10^6$ are depicted in Fig. 12(a and b).

5. Conclusions

Numerical computations are performed to study magnetoconvection in enclosures containing water near its maximum density in the presence of Soret and Dufour parameters. It is observed that the density inversion leaves strong effects on fluid flow, heat and mass transfer due to the formation of bi-cellular structure. The formation of dual cell structure and strength of each cell is always depends on the density inversion parameter, thermal Rayleigh number and Hartmann number. The heat and mass transfer rate behaves non-linearly with density inversion parameter and buoyancy ratio. The heat and mass transfer rate decreases with an increase of Hartmann number. The heat and mass transfer rates are found to increase with increasing thermal Rayleigh number. The mass transfer rate is decreased for high Hartmann number when increasing the thermal Rayleigh number. The heat transfer rate is minimum when $\phi = 0^o$, and maximum when $\phi = 90^o$ with increasing Hartmann number, but in the mass transfer rate behaves opposite. $D_f = 1$, $S_r = 0$ and $D_f = 0$, $S_r = 0$ gives better mass transfer rate and low heat transfer rate but the opposite of it holds for $D_f = 0.5$, $S_r = 0.5$ and $D_f = 0$, $S_r = 1$. The heat transfer rate increases and mass transfer rate decreases when the density inversion parameter increases in the presence of Soret and the absence of Dufour parameters.

Acknowledgments

The authors gratefully acknowledge the support provided to this study by the NCKU Project of Promoting Academic Excellence.

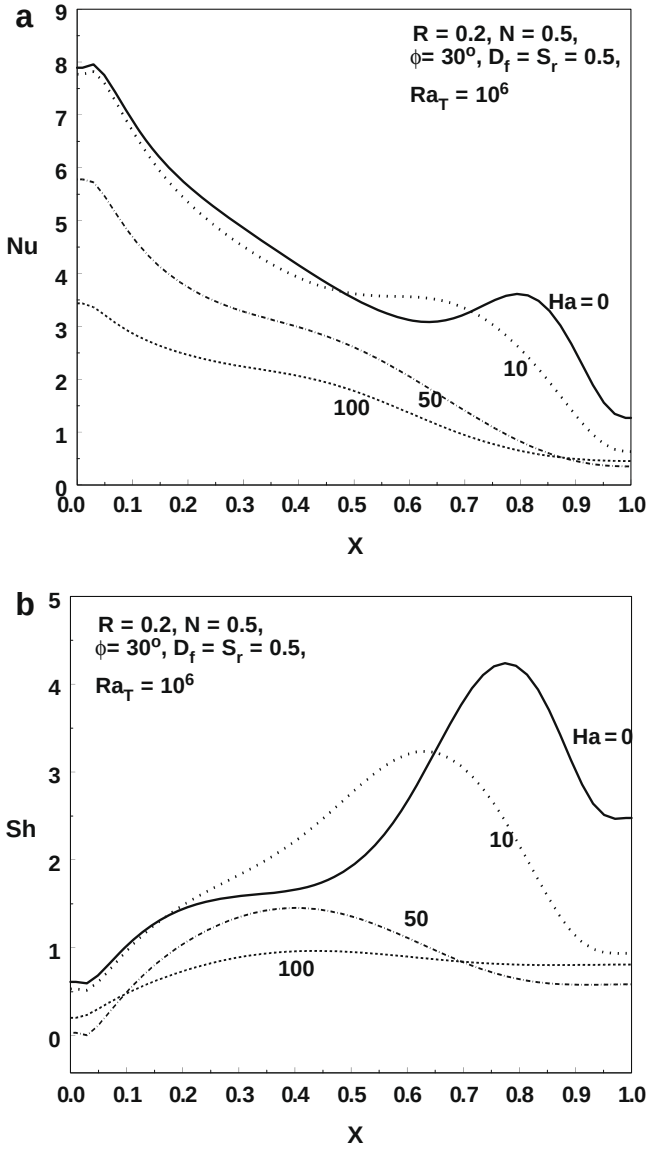

Fig. 12. (a and b) Local Nusselt number and Sherwood number for different Hartmann numbers, $R = 0.2$, $N = 0.5$, $\phi = 30^o$, $D_f = S_r = 0.5$ and $Ra_T = 10^6$.

References

[1] D.V. Davis, Natural convection of air in a square cavity: a benchmark numerical solution, Int. J. Numer. Methods Fluid 3 (1983) 249–264.

[2] A. Ostrach, Natural convection in enclosures, J. Heat Transfer 110 (1988) 1175–1190.

[3] D.S. Lin, M.W. Nansteel, Natural convection heat transfer in a square enclosure containing water near its density maximum, Int. J. Heat Mass Transfer 30 (1987) 2319–2329.

[4] M.W. Nansteel, K. Medjani, D.S. Lin, Natural convection of water near its density maximum in rectangular enclosure: low Rayleigh number calculations, Phys. Fluids 30 (1987) 312–317.

[5] W. Tong, J.N. Koster, Coupling of natural convection flow across a vertical density inversion interface, Warme. Stoffubertrag. 28 (1993) 471–479.

[6] W. Tong, Aspect ratio effect on natural convection in water near its density maximum temperature, Int. J. Heat Fluid Flow 20 (1999) 624–633.

[7] C.J. Ho, F.J. Tu, Transition to oscillatory natural convection of water near its density maximum in a tall enclosure, Int. J. Num. Methods Heat Fluid Flow 11 (2001) 626–641.

[8] M.A. Hossain, D.A.S. Rees, Natural convection flow of water near its density maximum in a rectangular enclosure having isothermal walls with heat generation, Heat Mass Transfer 41 (2005) 367–374.

[9] P. Kandaswamy, S. Sivasankaran, N. Nithyadevi, Buoyancy-driven convection of water near its density maximum with partially active vertical walls, Int. J. Heat Mass Transfer 50 (2007) 942–948.

[10] N. Nithyadevi, S. Sivasankaran, P. Kandaswamy, Buoyancy-driven convection of water near its density maximum with time periodic partially active vertical walls, Meccanica 42 (2007) 503–510.

[11] I. Sezai, A.A. Mohamad, Double diffusive convection in a cubic enclosure with opposing temperature and concentration gradients, Phys. Fluids 12 (2000) 2210–2223.

[12] E. Blums, Heat and mass transfer phenomena, J. Magn. Magn. Mater. 252 (2002) 189–193.

[13] I. Hajri, A. Omri, S. Ben Nasrallah, A numerical model for the simulation of double-diffusive natural convection in a triangular cavity using equal order and control volume based on the finite element method, Desalination 206 (2007) 579–588.

[14] S. Sivasankaran, P. Kandaswamy, Double diffusive convection of water in a rectangular partitioned enclosure with conductive baffle on hot wall, Arab. J. Sci. Eng. 32 (2007) 35–48.

[15] K.R. Singh, T.G. Cowling, Thermal convection in magnetohydrodynamics, Quart. J. Mech. Appl. Math. XVI (1963) 17–31.

[16] N. Rudraiah, R.M. Barron, M. Venkatachalappa, C.K. Subbaraya, Effect of a magnetic field on free convection in a rectangular enclosure, Int. J. Eng. Sci. 33 (8) (1995) 1075–1084.

[17] J. Qi, N.I. Wakayama, A. Yabe, Magnetic control of thermal convection in electrically non-conducting or low-conducting paramagnetic fluids, Int. J. Heat Mass Transfer 44 (2001) 3043–3052.

[18] A.J. Chamkha, H.A. Naser, Hydromagnetic double-diffusive convection in a rectangular enclosure with opposing temperature and concentration gradients, Int. J. Heat Mass Transfer 45 (2002) 2465–2483.

[19] M.A. Hossain, M.Z. Hafiz, D.A.S. Rees, Buoyancy and thermocapillary driven convection flow of an electrically conducting fluid in an enclosure with heat generation, Int. J. Thermal Sci. 44 (2005) 676–684.

[20] F. Joly, P. Vasseur, G. Labrosse, Soret-driven thermosolutal convection in a vertical enclosure, Int. Commun. Heat Mass Transfer 27 (2000) 755–764.

[21] A. Bahloul, N. Boutana, P. Vasseur, Double-diffusive and Soret-induced convection in a shallow horizontal porous layer, J. Fluid Mech. 491 (2003) 325–352.

[22] A. Postelnicu, Influence of magnetic field on heat and mass transfer by natural convection from vertical surfaces in porous media considering Soret and Dufour effects, Int. J. Heat Mass Transfer 47 (2004) 1467–1472.

[23] J.K. Platten, The Soret effect: a review of recent experimental results, J. Appl. Mech. 73 (2006) 5–15.

[24] A.J. Chamkha, A.B. Nakhi, MHD mixed convection radiation interaction along a permeable surface immersed in a porous medium in the presence of Soret and Dufour's effects, Heat Mass Transfer 44 (2008) 645–856.

[25] M.A. Ei-Aziz, Thermal diffusion and diffusion thermo effects on combined heat and mass transfer by hydromagnetic three dimensional free convection over a permeable stretching surface with radiation, Phys. Lett. A 372 (2008) 263–272.

[26] S.V. Patankar, Numerical heat transfer and fluid flow hemisphere, McGraw-Hill, Washington, DC, 1980.

[27] G.V. Hadjisophocleous, A.C.M. Sousa, J.E.S. Venart, Prediction of transient natural convection in enclosures of arbitrary geometry using a nonorthogonal numerical model, Numer. Heat Transfer 13 (1988) 373–392.

[28] M.C. Ece, E. Buyuk, Natural convection flow under a magnetic field in an inclined rectangular enclosure heated and cooled on adjacent walls, Fluid Dyn. Res. 38 (2006) 564–590.